applied sciences

MDPI

Article

Experimental Study and Phenomenological Laws of Some Nonlinear Behaviours of the Wheel–Rail Contact Associated with the Deshunting Phenomenon

Guy-Léon Kaza [1], Frédéric Houzé [2], Florent Loëte [2,*] and Philippe Testé [2]

[1] Département de la Signalisation Ferroviaire, SNCF Réseau, Direction Générale Industrielle & Ingénierie, 6 Avenue François Mitterrand, 93574 La Plaine Saint-Denis, France
[2] Laboratoire de Génie Électrique et Électronique de Paris, CNRS, CentraleSupélec, Université Paris-Saclay, 91192 Gif-sur-Yvette, France
* Correspondence: florent.loete@centralesupelec.fr

Abstract: A widely used technique for locating the position of a train during its journey involves electrical detection: on a section of track, the train closes ("shunts") a circuit dedicated to its location via its wheels and axles. The quality of the wheel–rail contact is therefore particularly important for signalling management and traffic control. In this paper, we show that the current flowing through the track circuit induces a permanent modification and a nonlinear, frequency-dependent behaviour of the electrical contact. We propose an analytical expression that describes the evolution of the measured voltage as a function of current and frequency for these nonlinear behaviours. This behavioural law was obtained using experimental measurements on a real train and could therefore be integrated into a global model describing the track system.

Keywords: wheel–rail contact; track circuit; deshunting; reliability

Citation: Kaza, G.-L.; Houzé, F.; Loëte, F.; Testé, P. Experimental Study and Phenomenological Laws of Some Nonlinear Behaviours of the Wheel–Rail Contact Associated with the Deshunting Phenomenon. *Appl. Sci.* **2023**, *13*, 11752. https://doi.org/10.3390/app132111752

Academic Editors: Zhipeng Wang, Yong Qin and Jie Geng

Received: 5 September 2023
Revised: 20 October 2023
Accepted: 24 October 2023
Published: 27 October 2023

1. Introduction

In many countries, most railway signalling functions require knowledge of the occupancy status of portions of track called "zones". This parameter is necessary for the efficient and safe planning of trains [1]. In a zone, the traffic and presence of trains is detected by means of a "track circuit". This consists of an emitter, a receiver, and a transmission line formed by the rails. If a train is present in the zone, the axles of the train "shunt" the signal transmitted by the emitter, and the presence of the train is then detected at the receiver. The reliable detection of the train by the track circuit is essential for triggering the signalling systems adequately and, consequently, ensuring the correct management of the railway systems.

However, track circuits have a fairly high failure rate. Chen et al. in the UK [2] and Wybo in France reported 47 incidents in 2016 [3]. The reliability of track circuits depends not only on the electronic circuit itself, but also on the quality of the electrical contact between the train wheels and the rails.

While factors such as dense traffic or heavy trains contribute to good wheel–rail contact, other factors have been identified as participating in its degradation. Among them, we can mention the possibility of bad ballasts (inducing leakage currents), too-light axle loads or inadequate tonnage, unsuitable wheel and track profiles, contamination (e.g., lost material from train freight, leaves, rubber residues, dirt, oxidation), no wheel scrubbers or disc brakes, sanding from locomotives, non-electric traction, low traffic, etc.

Much work has been carried out on the reliability of track circuits [2–5]. However, in most cases, these studies are based on the assumption of an ideally low and stable wheel–rail resistance. To make it so, effective "shunting" is essential and requires a good-quality electrical contact between the wheels and the rails to avoid "deshunting", which could

have serious consequences for the safety of traffic. But despite the importance of these electrical considerations, most of the studies focusing on the wheel–rail contact concern the problems of adhesion and wear [6–8].

1.1. Quick Reminder of the Properties of Wheel–Rail Electrical Contacts

The works concerning the electrical properties of wheel–rail contact are less numerous than those related to adhesion problems, for example. In this section, we present a brief state of the art on this subject. Usually, in the railway field, without considering the technological evolutions (e.g., weight reduction, etc.) that can also deteriorate the quality of the wheel–rail electrical contact, two types of factors may be distinguished that have an influence on it:

- The presence of what is called a "third body" between the two elements in contact.
- The existence of an oxidised layer.

The third body, present between the solid surfaces in contact, is mainly composed of particles detached from them (the wheel and the rail) and of contaminants (such as dead leaves, water, fragments of ballast stones, sand, oil, various pollutants, etc.), with a thickness from a few micrometres to several tens of micrometres on the rail and wheel [9]. The study of the role of the third body is particularly complex due to the permanent changes in the strongly related geometric and electrical properties of this interface material throughout the movement of the train [10]. Descartes et al. studied the influence of the compactness and heterogeneity of the third body on the shunting ability, and they observed that the characteristic of the third body that leads to poor shunting seems to be its heterogeneity.

Lewis et al. [11] conducted an experimental study to investigate the effect of sand-blasting on the electrical insulation of a wheel–rail contact. Indeed, the presence of sand can compromise the quality of the contact. Static and dynamic tests were performed. They observed a transition in the contact resistance according to the quantity of sand between the two elements. They proposed a model of electrical insulation by assuming either a total separation of the two metallic parts by a layer of sand, or a partial contact of the disc with a certain amount of sand. They also observed [12], for instance, that the larger the grain size of the sand, the less it affected the degradation of the wheel–rail contact.

Concerning problems related to surface oxidation, several studies have been conducted as early as 1960 [13–16] to better understand the shunting phenomena in the case of a stationary or moving train. These studies were carried out either at scale one or at smaller scales (e.g., cylinders rolling on one another or in a ball/plane configuration) to more precisely study the effect of an oxide layer on the contact, for example. From an electrical point of view, the injected signals corresponded either to those of the track circuit or to "laboratory" signals. The studies focused on two parameters: the contact resistance and the breakdown voltage (i.e., the voltage sufficient to allow the current to flow between the wheel and the rail). In the case of shunting at standstill on scale-one devices, and also on laboratory devices at a smaller scale (e.g., two cylinders rolling over one another), the studies showed that beyond a certain voltage the contact resistance sharply decreases. This voltage depends on various parameters, such as the time of application of the voltage, the contact pressure, and the degree of hygrometry. Moreover, the contact resistance and the breakdown voltage do not seem to be correlated a priori. The main results can be summarised as follows:

- The breakdown voltage depends on the contact pressure, the environmental conditions (oxidation, pollution), the contact surface, and the speed of movement.
- The measured contact resistance may show an irreversible change, which would correspond to a change of state in the contact.
- Time constants have been found in the evolution of the contact resistance and the breakdown voltage.

Indeed, it was observed that the current in an oxidised contact can only flow when the oxide layer is "cracked", since even a very thin oxide layer is sufficiently resistive to

create a high resistance. Thus, an oxide thickness of 100 Å is enough to create a "sheet resistance" of 10 Ω/square. For the current to pass, it is necessary to have "cracking" of the layer under the effect of a stress (mechanical, electrical, chemical, or thermal). Several phenomena leading to the passage of the current have been proposed. Among them, Holm [17] proposed two types of "fritting" phenomena:

- Type A fritting: After local melting, the metal fills the "cracks" and establishes the contact. This mode of fritting takes place for a large oxide thickness (greater than 50 Å). The film oxide film is slashed by the tension. This phenomenon is irreversible.
- Type B fritting: The conditions leading to fusion are not reached. This mode of fritting takes place for small oxide thicknesses (i.e., less than 50 Å). In this case, the oxide is pierced by the metallic roughness peaks that establish the electrical contact through "spots".

In 2008, Fukuda et al. [18] highlighted the role of the main parameters influencing the contact resistance. They studied the influence of the rail rust thickness, the roughness of the wheels, the car load, and the current flowing in the track circuit. They quantified how the rust thickness depends on environmental conditions (e.g., industrial, seaside, rural, or mountain sites) and on the density of rail traffic. The influence of these parameters was then studied on lab equipment simulating realistic wheel–rail contact conditions at low speeds.

In 2012, measurements of the electrical behaviour of a wheel–rail contact were performed both on a 1:4-scale laboratory bench and on an instrumented car on a real track [19]. These measurements of contact current and voltage were made in view of a statistical approach that highlighted the typology of the *I–V* curves. Thus, both in the laboratory and on the outdoor site, nonlinear *I–V* characteristics were observed for various values of mechanical loads and speeds. The nonlinearity is all the more important when the wheel or rail surfaces are oxidised.

Moreover, saturation in the *I–V* characteristics occurs for values in the range of 0.4–0.6 V, which does not depend on the current intensity through the contact. This leads to an irreversible transition in the behaviour of the contact (when the train is stopped). An interpretation of this phenomenon has been proposed based on an electrothermal process in granular media (the Branly effect) [20].

Among the works concerning the study of wheel–rail contact resistance in degraded conditions, we can cite [21,22]. The authors introduced the notion of imperfect contact. They attributed the degradation of resistance to a very thin but robust and stable oxide film, rich in chromium. This contact has a highly variable resistance when the voltage varies. According to the authors, this resistance evolves in an irreversible way when the voltage increases because of a very fast electrical breakdown followed by a thermal breakdown.

In addition, various approaches have been proposed to take into account the degradation of the wheel–rail contact. In [23], the authors studied the influence of the degree of pollution on wheel–rail contact resistance under static conditions. They defined three different degrees: a clean contact state, and two polluted states, which result in a multiplication of resistance by a factor of 1–5 for degree one and a factor of 6–10 for degree two. These coefficients are given by a normal statistical distribution law. In [24], the authors introduced oxidised wheel–rail contact in the form of an additional capacitor in the track circuit. In [25] the authors considered that the oxidised contact behaves like a semiconductor, either like a diode or a transistor.

1.2. Objectives and Organisation of the Paper

The work presented hereafter aims at proposing a model of wheel–rail contact that can be integrated at the level of the track system. It is a question of associating the contact with a behavioural law allowing the contact to be described by a characteristic $U = f(I, f)$. This behavioural law is obtained from nonlinear $U(I)$ curves observed at scale one and on the 1:4-scale bench, as mentioned above. We were particularly interested in the influence of

an oxide layer (one of the elements likely to constitute the third body, in this case formed intentionally) on the behaviour of the contact impedance, and we also sought to estimate the dependence of this contact impedance on the frequency of the injected signal. The rest of this paper is organised as follows:

- Section 2 is dedicated to the description of the reduced-scale experimental setup implemented. This setup, already described in [19], is briefly recalled, and the preparation of the surfaces of the wheel and rail models and the method for electrical measurements are detailed. The main results focused on the influence of the intensity and frequency of the injected current are reported.
- Then, Section 3 proposes a comparative analysis of the results between the reduced-scale and full-scale tests. It then discusses different analytical expressions fitting the experimental curves observed at both scales, which can be used as behavioural laws.
- Finally, Section 4 discusses the behaviour of the voltage–current characteristic curves in the presence of an oxide layer, and especially the irreversible evolution linked to the maximum current flowing through the contact.

2. Experiments on a Reduced-Scale Laboratory Bench

2.1. Mechanical Experimental Setup

The general principal of the detection of a train by a real-life track circuit is shown in Figure 1. An emitter sends a time-dependent signal down a transmission line formed by the rails. If a train is present between two consecutive pairs of insulated joints, the axles of the train "shunt" the signal transmitted by the emitter. If the recorded signal is below a predefined threshold, the train is considered to be present in the section.

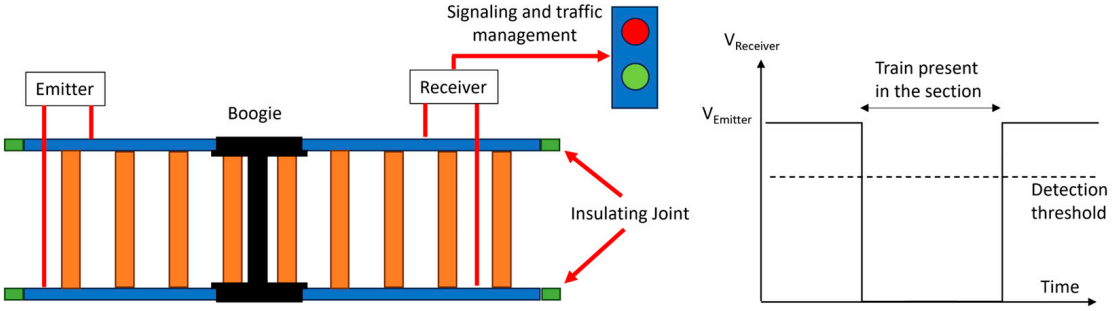

Figure 1. General principle of train's detection by a track circuit.

The mechanical part of the experimental setup, developed by H. Chollet et al. at the French Institute of Science and Technology for Transport, has been described in detail in reference [19]. We can simply recall that the reality of a railway axle standing on its rails is simulated by "wheel" and "rail" elements of simplified geometry, made at 1/4 scale from steels identical to those of the real elements. Size reduction follows precise similarity laws based on mechanical considerations. Rolling tests can mimic travel at a linear speed of a few km/h, with a normal load corresponding to the weight per axle of a real wagon, applied to the experimental wheelset via a pneumatic jack. In the present study, we aim to be representative of rolling stock characterised by a load per axle of 12.4 tons, which translates on the scaled model into an applied vertical load of 7.7 kN.

2.2. Preparation of Steel Surfaces

The running surfaces of the model's wheels and rails were prepared in such a way as to have, on the one hand, a "sound" state serving as a reference, and on the other hand, a "degraded" state intended to reproduce the deterioration undergone by the rolling stock in service.

In the first case, the rail surface was ground and brushed to a shiny finish, while the wheel surface was left with its slight natural oxidation.

In the second case, a specific oxidation protocol (described in [19]) was used to impose accelerated rusting of the rail surface, which was then dried and compacted by rolling. The average thickness of the oxide layer that formed was assessed by a magnetic inductive method at 5.9 µm (standard deviation of 0.86 µm) in the tread, and 41.9 µm (standard deviation of 8.75 µm) on either side of it.

2.3. Adaptation for Electrical Measurements

Finally, the device was adapted to perform contact resistance measurements at both wheel–rail contacts using the four-probe method. The rails were electrically insulated from the frame by interposing a Kapton film. For each side, current supply and voltage measurements were performed using copper brushes pressed against the inside of the wheel and rail, as schematically shown in Figure 2. For the experiments reported in this paper, we used a low-frequency generator associated with a voltage supply (20 V max). Current intensity was determined through the measurement of the voltage drop at a 1 Ω resistor terminals; its maximum value was about 6 A.

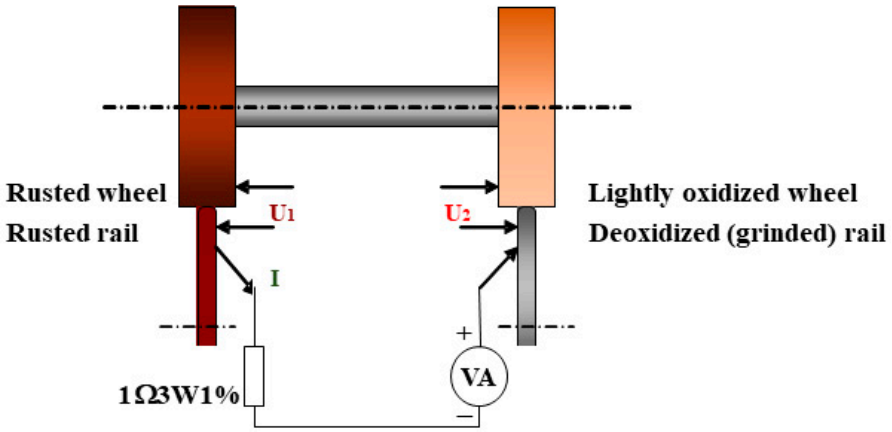

Figure 2. Principle of the electrical contact resistance measurement the by four-probe method; on the (**left side**), intentionally rusted surfaces; on the (**right side**), "clean" reference surfaces. Black arrows represent copper brushes for measurements of current feeding (**bottom**) and contact voltages (U_1 and U_2).

2.4. Results

As already mentioned in the Introduction, in this article we focus only on static tests. For each case, we will consider representative voltage–current characteristics taken over a few periods.

2.4.1. Influence of the Current Intensity

In a previous study carried out by the SNCF under railway conditions (i.e., at scale one), it was observed that the highest track circuit current intensities caused an irreversible modification of the electrical behaviour of the wheel–rail interface (for the usual frequency of 2300 Hz). We therefore sought to reproduce this effect on the bench. In order to achieve this goal, for the same frequency of 2300 Hz, we first imposed current intensities of 1.25, 3.7, and 5.2 A before applying a maximum intensity of 6.3 A; finally, the initial intensities were applied again. The corresponding characteristics are presented in Figure 3. The curve relating to the maximum current is plotted with black symbols, while the curves relating to the other currents are plotted with coloured symbols—blue before the maximum current is imposed, and red after. We can see first that all of the curves are nonlinear, which was also observed during tests at scale one as soon as the current was higher than 1 A. But we can see above all that, whatever the current applied, the curves obtained after the maximum current intensity sequence are superimposed on the characteristic relating to the latter. This attests to an irreversible modification of the interface by the highest current intensity.

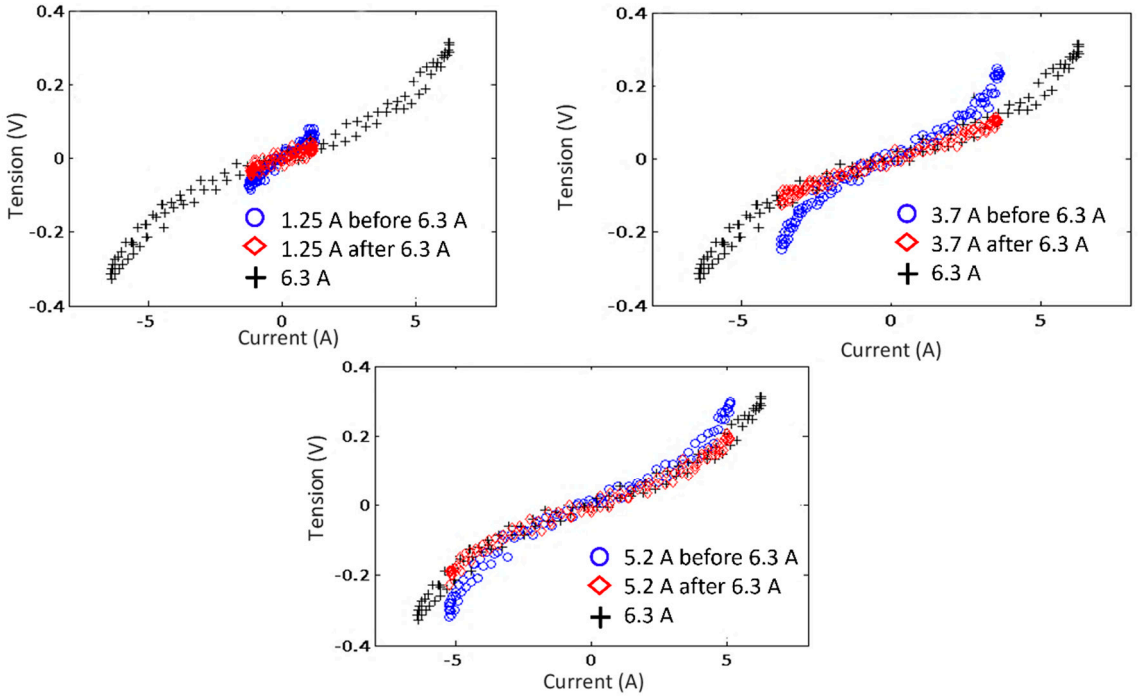

Figure 3. Comparison of voltage–current characteristics (over a few periods) measured before and after a sequence at maximum intensity of 6.3 A, for three different current values (signal frequency: 2300 Hz).

2.4.2. Influence of the Frequency

To study the influence of the frequency, we chose to consider two current values: one below 1 A, leading to nearly ohmic characteristics (800 mA), and the other above 1 A, to observe nonlinear behaviours (6 A). Three frequency intervals were chosen: 230 Hz–1.8 kHz, 2.3 kHz–18 kHz, and 23 kHz–40 kHz, with four frequency values considered in each. The results of these tests are presented in Figures 4 and 5. In the first case (I_{max} = 800 mA), the characteristics are quasilinear, with identical slopes for 230 Hz and 2.3 kHz, and then hysteresis starts to appear for 23 kHz, with the average slope remaining approximately the same. In the second case (I_{max} = 6 A), the characteristics are clearly nonlinear. Quasi-superimposable up to 9 kHz; they then show an increasingly pronounced hysteresis as the frequency increases. At the highest frequencies, the tension–current characteristic evolves towards a shape close to an ellipse, together with a slight decrease in the maximum voltage.

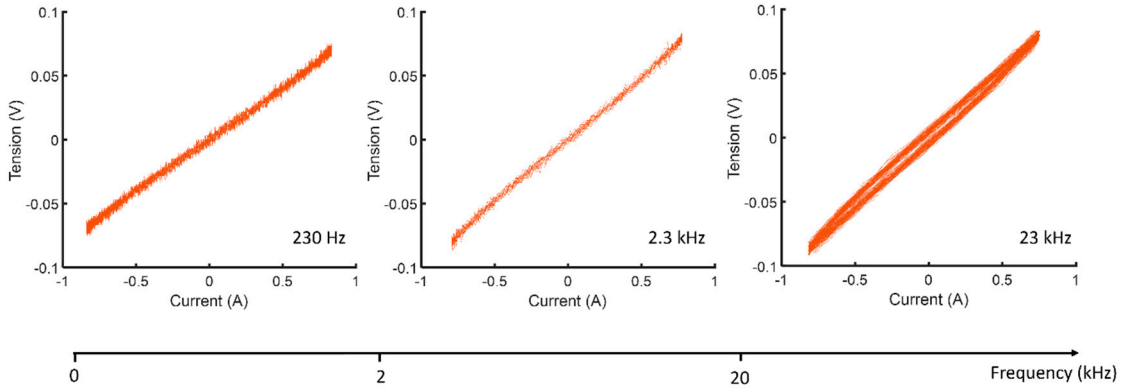

Figure 4. Comparison of voltage–current characteristics (over a few periods) for 3 frequency values, for a maximum current intensity of 800 mA.

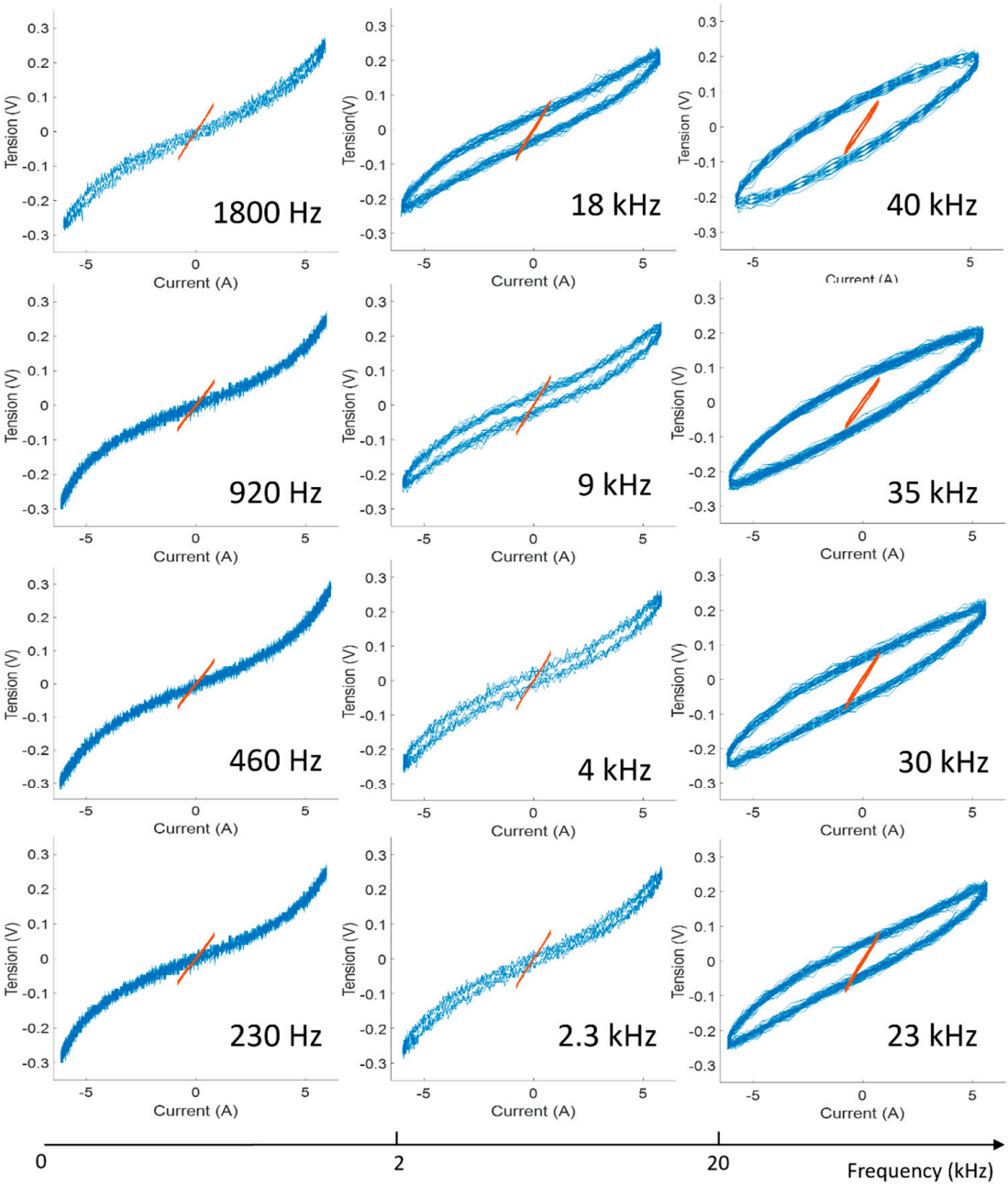

Figure 5. Comparison of voltage–current characteristics (over a few periods) measured for various frequency values from 230 Hz to 40 kHz, for a maximum current intensity of 800 mA (red curves) and 6 A (blue curves).

3. Full-Scale Experiments on a Real Train and Proposition of Behavioural Laws

After carrying out the investigations described in Section 2, our goal was focused on correlating the nonlinear behaviour observed on a reduced scale with that of a real-life experiment. Finally, on the basis of the similar behaviours observed, we developed and tested an electrical behavioural law for the wheel–rail contact. Knowledge of such a law could be very useful to railway engineers when facing the deshunting phenomenon or designing new transportation systems.

3.1. Full-Scale Experimental Setup

A wheel–rail contact resistance measurement campaign was carried out by the SNCF using a specially instrumented railcar on a straight section of track in Normandy, charac-

terised by low traffic levels of just a few trains per day. Power was supplied via the track circuit. The experimental device, described in [19], was installed in front of one of the wheels on the railcar's front axle. Using copper rollers applied to the wheel and the rail, it measures the wheel–rail voltage drop both at standstill and when the train is moving at low speed. Current intensity is measured using a Rogowski coil around the axle's axis. Successive series of electrical data were recorded as the train moved slowly (~1 m/s) along a 100 m section of line. Prior to the tests, a few-meter section of rail was brushed and degreased to provide a "clean rail" reference.

3.2. Electrical Behavioural Law at 230 Hz and 2300 Hz

Interestingly, the nonlinear behaviour and hysteresis phenomenon observed at a reduced scale, as shown in Section 2 (Figure 5), were also witnessed in the railway site tests under real conditions, as one can see in Figures 6 and 7. One can note that the nonlinearity is slightly less pronounced compared to the 6 A curves pictured in Figure 5, since the track circuit only allowed a current of 2 A to flow. The voltage current characteristics in this real case are therefore in between those obtained with the laboratory bench. Consequently, it was deemed interesting to investigate which behavioural law could fit those data to serve as a model for railway engineers.

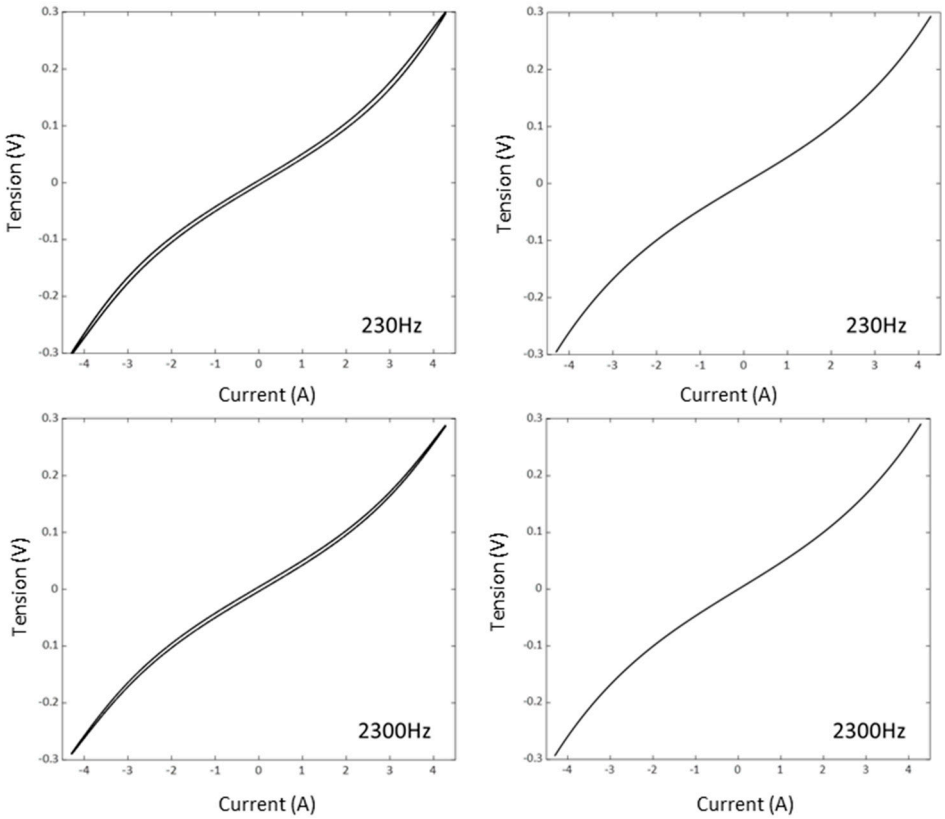

Figure 6. Comparison between the experimental results (**left**) for $I = 3$A and the proposed nonlinear model (**right**) for the $U = f(I)$ characteristics at $f = 230$ Hz (**above**) and $f = 2300$ Hz (**below**).

For each frequency and intensity, a nonlinear regression of $U = f(I)$ was performed over several periods, containing around 2 million points. It was found empirically that the tension–current curves could be satisfyingly approximated by the following nonlinear law:

$$U = a\,exp(bI) + c\,exp(dI) \quad (1)$$

where a, b, c, and d are the regression parameters, while U and I are the contact tension and the current through the contact, respectively. The nonlinear regression was carried out using the nonlinear least-squares solver function in MATLAB (R2022b).

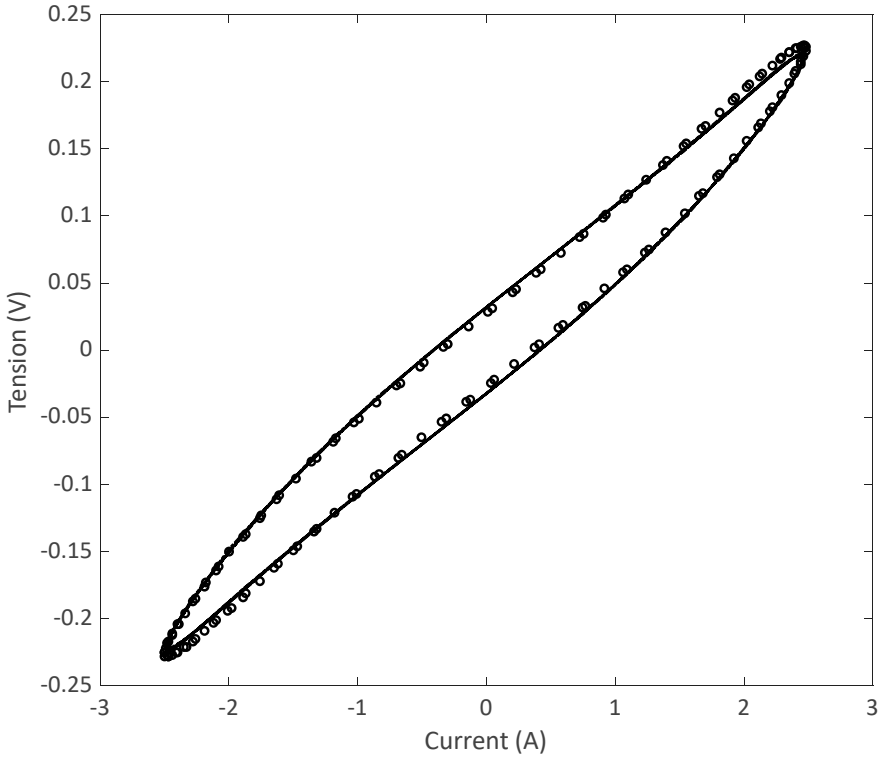

Figure 7. Comparison between the experimental results (**o**) and the fitted data (**-**) using our hysteresis model at 23 kHz for I = 2 A.

In practice, it was found that $c \cong -a$ and $d \cong -b$; consequently, (1) can be simplified as follows:

$$U = 2a \sinh(bI) \tag{2}$$

Figure 6 shows how, at low frequencies (230 Hz and 2300 Hz), the nonlinear model proposed in (2) accurately fits the experimental $U = f(I)$ series. The estimated coefficients a and b are given in Table 1. The experimental series chosen in this example exhibit very similar behaviour to those in Figure 3.

Table 1. Coefficients of the fitting law for I = 3 A.

f (Hz)	a	b
230	0.0588	0.3844
2300	0.06148	0.3728

3.3. Electrical Behavioural Law at 23 kHz

The methodology introduced in the previous section had to be modified, since in the case of a tension–current characteristic without hysteresis we made the assumption of a contact simply modelled by a variable resistance. Therefore, at higher frequencies, an inductive contribution had to be introduced to account for the experimentally observed hysteresis effect. The first step consisted of estimating the resistive part with (2). The inductance was estimated in a second step via the following method:

- The cycle was separated into two fronts (rising and descending);
- Each front was adjusted with the empirical model described previously:

$$U_{r,d} = a_{r,d}\exp(b_{r,d}I) + c_{r,d}\exp(d_{r,d}I) \quad (3)$$

where the subscripts r and d represent the rising and decreasing phases of the cycle, respectively.

Using the following expressions, we found that the quantities $U_{r,d} - 2a\sinh(bI)$ and $\frac{dI}{dt}$ can be considered proportional, since their ratio is constant over a wide range. Therefore, one can write

$$U = 2a\sinh(bI) + L\frac{dI}{dt} \quad (4)$$

The estimated coefficients are given in Table 2. As one can see in Figure 7, this model fits the experimental data at 23 kHz with fairly good agreement. This model can be easily extended for modelling at other frequencies.

Table 2. Coefficients of the fitting law with hysteresis at 23 kHz.

I_{eff}	a	b	L
2 A	0.099	0.394	9.05×10^{-8}
3 A	0.066	0.362	7.4×10^{-8}

4. Discussion of *U(I)* Curves in the Case of an Oxidised Fixed Contact

It is interesting to study the influence of the peak value of the current injected into the contact. To do this, we will distinguish two cases presented in Figure 8: two current sinusoidal waves of the same frequency, but with different peak current values (I_{max}): $I_{max1} < I_{max2}$. The figure also distinguishes the first period (solid line) from the subsequent periods (dashed lines).

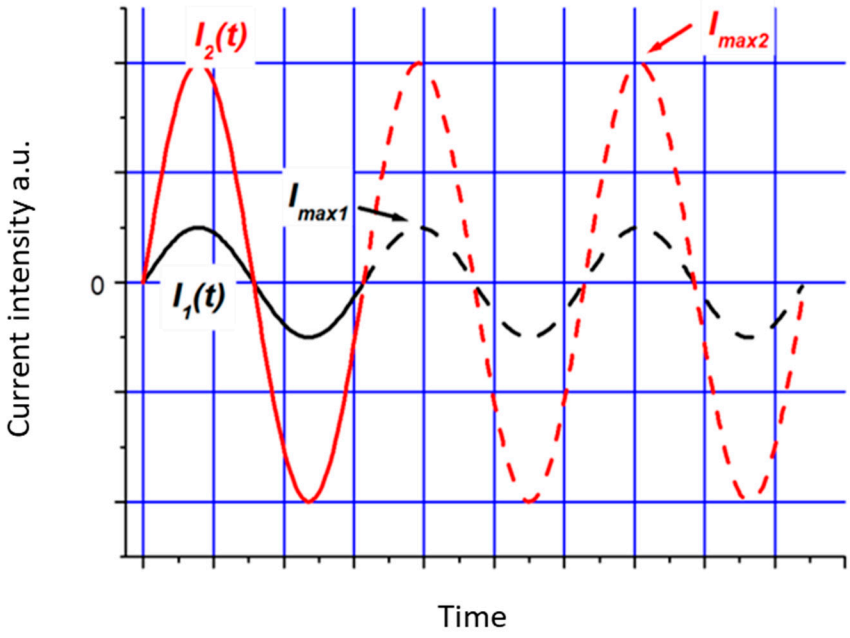

Figure 8. Schematic representation of the two cases studied: $I_1(t)$: current wave with a "low" maximum value; $I_2(t)$: current wave with a "high" maximum value. In both cases, the first period is shown as a solid line and the following periods are shown as dashed lines.

4.1. Case of a Low Peak Current

In this case, we plotted the contact voltage in arbitrary units against the instantaneous value of the current, as shown in Figure 9. This curve is valid both for the first current period and during the steady state (i.e., the following periods). An increase in voltage

corresponding to a "high" contact resistance is observed, which is independent of the current value. The curve is approximately symmetrical: the maximum values of the voltages U_{c1} and U'_{c1} seem to be opposite to one another. The current flow does not seem to have any influence on the contact resistance (i.e., on the size and nature of the contact area).

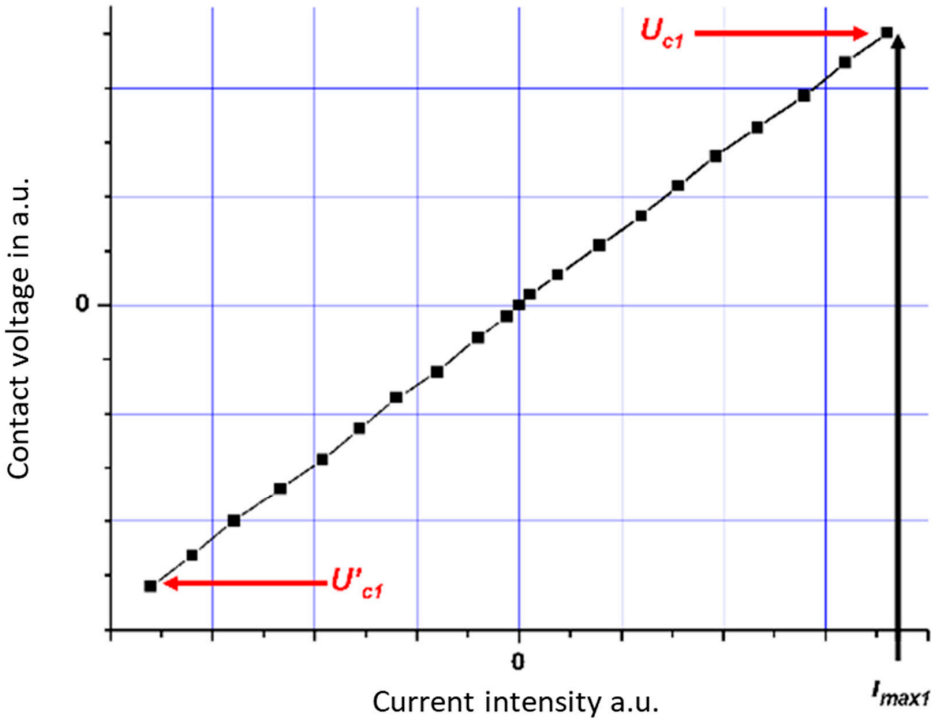

Figure 9. Qualitative representation of the variation in the contact voltage with the current intensity for a current wave of "low" peak intensity. The figure is valid for the first and subsequent current periods.

4.2. Case of High Peak Intensity

It is interesting to distinguish the first period from the subsequent ones.

4.2.1. Phenomena Observed during the First Period

In Figure 10, we have plotted the contact voltage (in arbitrary units) as a function of the instantaneous value of the current intensity (also in a.u.) during the first current period. Several phases can be seen on this *U(I)* curve:

- Phase 1 (in blue): An increase in the contact voltage associated with a high contact resistance. The value of the contact resistance is almost independent of the current value.
- Phase 2 (in red): Above a certain value of the current, the contact resistance ($U(t)/I(t)$) decreases and a nonlinear behaviour appears. This can be interpreted as an increase in the contact area due to local softening in connection with Joule-effect heating. A change in the nature of the material within the contact area is also possible. This phase starts during the increase in $I(t)$ and continues during the decrease in $I(t)$.
- Phase 3 (in green): Below a certain value of the current, the voltage varies almost linearly with the current. During this phase, the heating of the contact zone is no longer sufficient to continue to modify it.
- Phase 4 (in orange): This phase includes the second half-period of the first alternation ($I(t) < 0$). The voltage evolutions are quite similar to those observed during the first three phases. When the current intensity increases in absolute value, heating is generated, which modifies the contact zone, always in the way of a decrease in contact resistance. When the current intensity increases again, ($I(t)$ tends towards 0),

the Joule effect is insufficient to modify the size and nature of the contact zone, and the dependence of the voltage on the current intensity becomes linear again.

- During the first period of the current there is therefore an irreversible evolution of the contact, which tends to decrease the contact resistance.

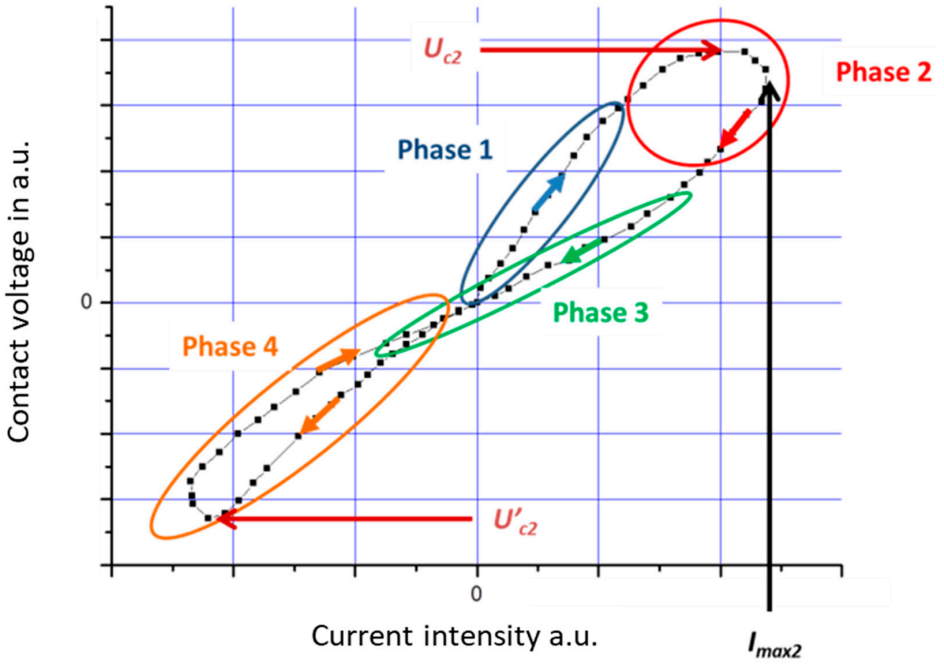

Figure 10. Qualitative representation of the different phases observed when the contact voltage varies with the current intensity during the first alternation of a current wave of high peak intensity. Colored arrows indicate how the curve is drawn.

4.2.2. Phenomena Observed during the Following Periods (Steady State)

In Figure 11, we can see on the one hand the *U(I)* characteristic for the first period (in black), and on the other the *U(I)* characteristics in steady state (in red).

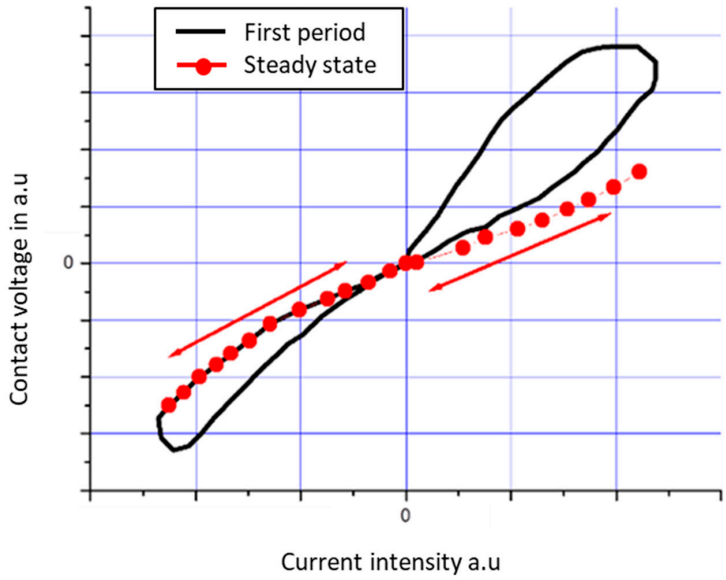

Figure 11. Qualitative representation of the contact voltage with the current intensity during the first (black) and the subsequent (red) periods of a current wave of high peak intensity (double arrows indicate reversibility).

Several Remarks

- The *U(I)* characteristic becomes repeatable over the periods. We have a steady state. This can be interpreted as indicating that the contact zone no longer varies over time due to the Joule effect.
- The branch at $I(t) < 0$ is superimposed on the end of the characteristic of the first period (i.e., the return part of phase four), which seems to indicate that the contact zone "changes" mainly during the first period. It stabilises on the lowest values of the contact resistance.
- The repeatable characteristic is not linear. At high values of *I(t)*, the contact resistance seems to increase, which can be explained by an increase in the resistivity value of the material within the zone. However, this variation in resistivity seems to be reversible.

When the sinusoidal current frequency increases, the appearance of a hysteresis cycle cannot yet be explained. An estimate shows that it is not due to the inductive effect of the current loop formed by the measuring circuit.

5. Conclusions

In this study, it was found that the wheel–rail contact has a clearly non-ohmic behaviour, contrary to what one might expect. The measurements were performed on a 1:4-scale laboratory bench. The recorded voltages at different frequencies and current intensities, over thousands of signal periods, allowed us to emphasise some very peculiar behaviours.

It was observed that during the very first periods of the current flowing through the contact, a permanent modification was induced, resulting in a reduced contact resistance, closer to ohmic behaviour. Furthermore, nonlinear characteristics were observed and a frequency-dependent hysteresis phenomenon was evidenced. Those observations emphasise the major security issue where the electrical wheel–rail contact may exhibit higher impedance during the first periods of the signal, resulting in the problematic non-detection of a train.

The physics behind these phenomena is not yet clear, and preliminary explanations have been discussed in this paper. Nonetheless, it is still important from the traffic and safety management point of view to be able to cope with this behaviour, since similar observations were found in real railway conditions. Consequently, analytical behavioural laws have been proposed to account for them, and they could be integrated in further work to improve the reliability of the detection systems.

Further investigations are in progress on the basis of a more sophisticated setup in order to better control all of the influencing physical parameters, and especially to understand the role of the oxidation state of the surfaces in both the static contact and the rolling contact.

Author Contributions: Investigation, data analysis and writing: G.-L.K., F.H., F.L. and P.T. All authors have read and agreed to the published version of the manuscript.

Funding: This work was carried out within the framework of projects financed by the Société Nationale des Chemins de Fer français (SNCF).

Institutional Review Board Statement: Not applicable.

Informed Consent Statement: Not applicable.

Data Availability Statement: Data unavailable due to privacy restrictions.

Acknowledgments: We are particularly grateful to Hugues Chollet (Institut Français des Sciences et Technologies des Transports, de l'Aménagement et des Réseaux, IFSTTAR) for providing us with the 1/4-scale experimental bench. We would also like to thank Xavier Lorang and Emmanuelle Guillaume, who supervised these projects, for their many technical and scientific exchanges.

Conflicts of Interest: The authors declare no conflict of interest.

References

1. Shakibayifar, M.; Hassannayebi, E.; Mirzahossein, H.; Zohrabnia, S.; Shahabi, A. An integrated train scheduling and infrastructure development model in railway networks. *Sci. Iran.* **2017**, *24*, 3409–3422. [CrossRef]
2. Chen, J.; Roberts, C.; Weston, P. Fault detection and diagnosis for railway track circuits using neuro-fuzzy systems. *Control Eng. Pract.* **2008**, *16*, 585–596. [CrossRef]
3. Wybo, J.L. Track circuit reliability assessment for preventing railway accidents. *Saf. Sci.* **2018**, *110*, 268–275. [CrossRef]
4. Oukhellou, L.; Debiolles, A.; Denoeuds, T.; Aknin, P. Fault diagnosis in railway track circuits using Dempster–Shafer classifier fusion. *Eng. Appl. Artif. Intell.* **2010**, *23*, 117–128. [CrossRef]
5. Zhao, L.H.; Wu, J.P.; Ran, Y.K. Fault diagnosis for track circuit using AOK-TFRs and AGA. *Control Eng. Pract.* **2012**, *20*, 1270–1280.
6. Li, Z.; Arias-Cuevas, O.; Lewis, R.; Gallardo-Hernandez, E.A. Rolling-sliding laboratory tests of friction modifiers in leaf contaminated wheel-rail contacts. *Tribol. Lett.* **2009**, *33*, 97–109. [CrossRef]
7. Omasta, M.; Machatka, M.; Smejkal, D.; Hartl, M.; Krupka, I. Influence of sanding parameters on adhesion recovery in contaminated wheel–rail contact. *Wear* **2015**, *322–323*, 218–225. [CrossRef]
8. Arias-Cuevas, O.; Li, Z.; Lewis, R. A laboratory investigation on the influence of the particle size and slip during sanding on the adhesion and wear in the wheel–rail contact. *Wear* **2011**, *271*, 14–24. [CrossRef]
9. Descartes, S.; Desrayaud, C.; Niccolini, E.; Berthier, Y. Presence and role of the third body in a wheel–rail contact. *Wear* **2005**, *258*, 1081–1090. [CrossRef]
10. Descartes, S.; Renouf, M.; Fillot, N.; Gautier, B.; Descamps, A.; Berthier, Y.; Demanche, P. A new mechanical–electrical approach to the wheel-rail contact. *Wear* **2008**, *265*, 1408–1416. [CrossRef]
11. Lewis, R.; Dwyer-Joyce, R.S.; Lewis, J. Wheel/rail contact isolation due to track contamination. In Proceedings of the 6th International Conference on Contact Mechanics and Wear of Rail/Wheel Systems (CM2003), Gothenburg, Sweden, 10–13 June 2003.
12. Arias-Cuevas, O.; Li, Z.; Lewis, R. Investigating the Lubricity and Electrical Insulation Caused by Sanding in Dry Wheel–Rail Contacts. *Tribol. Lett.* **2010**, *37*, 623–635. [CrossRef]
13. Garde, A. *Etude du contact électrique « rail-roue »*, Travail de fin d'études, Ecole Nationale des Ponts et Chaussées. 1976.
14. Righi, R.; Pannaria, F. Question A4 *Sensibilité au shuntage des circuits de voie—Principes scientifiques du contact électrique entre deux corps solides comportant des surfaces oxydées*. Internal report of the ''Office de Recherches et d'Essais de l'Union Internationale des Chemins de fer'': Utrecht; 1960.
15. Question A4 *Sensibilité au shuntage des circuits de voie*. Final report of the ''Office de Recherches et d'Essais de l'Union Internationale des Chemins de fer'': Utrecht. 1962.
16. *Aptitude au shuntage des CdV après stationnement prolongé de voitures équipées de seuls freins à disque*, Internal tests report of SNCF's IG.LE department: Saint-Ouen. 1991.
17. Holm, R. *Electric Contacts—Theory and Applications*; Springer: Berlin/Heidelberg, Germany, 2000.
18. Fukuda, M.; Terada, N.; Ban, T. Study of quantifying and reducing electrical resistance between wheels and rails. *QR RTRI* **2008**, *49*, 158–162. [CrossRef]
19. Houzé, F.; Chollet, H.; Testé, P.; Lorang, X.; Loëte, F.; Andlauer, R.; Debucquoi, S.; Lerdu, F.; Antoni, M. Electrical behaviour of the wheel-rail contact. In Proceedings of the 26th International Conference on Electrical Contacts (ICEC 2012), Beijing, China, 14–17 May 2012.
20. Falcon, E.; Castaing, B. Electrical conductivity in granular media and Branly's coherer: A simple experiment. *Am. J. Phys.* **2005**, *73*, 302–307. [CrossRef]
21. Zanwu, H.; Kairui, J.; Lingyao, S. The Mechanism of the Contact Resistance between Rail and Wheel in Bad Shunting Area. *Appl. Mech. Mater. Online* **2012**, *229–231*, 565–570. [CrossRef]
22. Zhang, Z.; Shi, M.; Wang, R. Analysis and Research on Poor Shunting of Track Circuits in High-speed Railway Stations Based on Computer Technology. *J. Phys. Conf. Ser.* **2020**, *1648*, 42023. [CrossRef]
23. Dimitrov, R. On the Impact of the Characteristics of Rolling Stock on Shunting Resistance of Rail Circuit. *World Transp. Transp.* **2018**, *16*, 50–69. [CrossRef]
24. Razgonov, A.; Zhuravlyov, A.; Yashchuk, K.; Shcheka, V. Investigation of train shunt problem in track circuits of signalling and interlocking devices. *MATEC Web Conf.* **2019**, *294*, 3007. [CrossRef]
25. Toyoma, T.; Fukuda, M.; Owada, K.; Fujita, H. Modeling for Semiconductor Characteristics of Electrical Contact Resistance between Rail and Wheel. *IEICE Tech. Rep.* **2012**, *112*, 157–162.